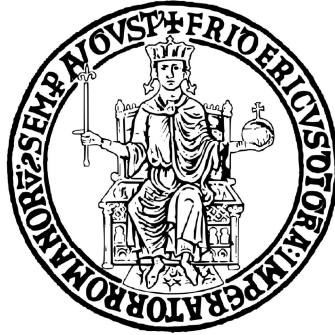


University of Naples Federico II



Department of Industrial Engineering

Ph.D. Programme in Industrial Engineering

XXXV Cycle

Ph.D Thesis

CFD-BASED ANALYSIS AND DESIGN OF DUCTED WIND TURBINES

Supervisors:

Ch.mo. Prof. Marcello Manna

Dr. Rodolfo Bontempo

Candidate:

Enrico Marco Di Marzo

Thesis submitted in 2023

Abstract

Wind conversion systems play an important role in the clean energy transition. However, these devices are characterised by low power density so that the rotor diameters are continuously increased to generate more power and to reduce the energy loss. In the last decades, several new off-shore wind plants have been designed to reduce the impact on the surrounding landscape, and different harvesting solutions have been proposed, such as small-scale wind turbines. The latter result in a very convenient solution since the energy is directly produced near the end-user, supporting the local grid. In this scenario, ducted wind turbines are very promising since they overcome some of the open rotor limitations. Indeed, the surrounding convergent-divergent nozzle increases the ingested mass flow rate, thanks to its cross-circulation, thus increasing the power output.

This work aims at designing a ducted wind turbine by defining a new design methodology based on optimization algorithms. Firstly, the weakness of the common practice of ducting an existing rotor is analysed by means of 3D blade-resolved CFD simulations. The NREL Phase VI rotor is enclosed within the Selig S1223 airfoil, whose stagger angle has been chosen to maximize the ingested mass flow rate. Despite both the rotor and the duct work in off-design conditions, the power coefficient of the shrouded case is higher than the open rotor value, even if the exit area is assumed as reference. However, in the latter case, the Betz-Joukowski limit is not exceeded.

However, it has been recently showed that DWTs can overcome this limit, even when the duct exit area is used as reference. Therefore, the CFD-AD methodology is extended to deal with ducted rotor, aiming at performing an iterative design via optimization, due to its low computational cost and its intrinsic ability to predict the duct-rotor interaction. Particularly, the results of the 3D CFD simulations are employed to tune the parameters involved in the actuator disk models. By doing so, the model is able to successfully predict the flow-field and the integral parameters of the two considered test-cases.

Once a fast and reliable tool is validated, the uncoupled and coupled design strategies are investigated. In the former, the duct is firstly optimized to maximize the ingested mass flow rate and, then, the disk load is chosen to maximize the power coefficient based on the exit area ($C_{P,ex}$). In the second case, the entire device is optimized contemporarily to maximize $C_{P,ex}$. Due to the lack of an optimal rotor distribution for the ducted case, the turbine, modelled as an actuator disk, consists in a free-vortex load (Joukowski rotor) along the whole span. The computed $C_{P,ex}$ exceeds the Betz-Joukowski limit only when a coupled design is carried out.

Abstract

Finally, the design of a novel ducted wind turbine is achieved by completely parametrizing the duct shape with Bezier curves, whose control points are defined by 8 geometrical design variables, such as the inlet and outlet metal angles, the leading edge radius, and the wedge angles, to mention few. Additionally, in order to reduce the load near the hub and the tip, a modified Shen's model is calibrated to match the CFD-3D data and it is introduced within the analysis module of the optimization procedure. The resulting DWT achieves a final $C_{P,ex}$ value of 0.604, exceeding the Betz limit.

Acknowledgments

First of all I would like to thank my supervisors Prof. Marcello Manna and Dr. Rodolfo Bontempo for guiding me through these three years, providing always useful suggestions and critical thoughts regarding the methodology and the approach.

Thanks also to Dr. Alessandro Cappiello for sharing with me parts of our paths, including all the interesting exchanges of ideas on our researches. I also would like to thank Antonio, Francesco, Ivano, Lorenzo and Ludovico for their never-ending long-distance encouragement and support.

My appreciation also goes out to my whole family for their encouragement and support all through my studies. An endless thanks goes to my father, my mother and my sister for all they have done for me up to now, I will be forever grateful. Finally, I would like to thank Laura for being by my side during all these years and for all her invaluable support.

Contents

Abstract	i
Acknowledgment	iii
List of Figures	v
List of Tables	ix
Nomenclature	ix
Introduction	0
1 A critical analysis of ducting an existing open rotor	8
1.1 Introduction	8
1.2 Grid generation strategy and description of the numerical set-up	10
1.3 Validation	13
1.3.1 Open Wind Turbine	13
1.3.2 Ducted wind turbine	16
1.4 Results	17
1.4.1 Comparison in terms of rotor and duct operating conditions	19
1.4.2 Comparison in terms of global performance coefficients and wake development	25
1.5 Conclusions	28
2 Assessment of the AD methodology for DAWTs	29
2.1 Introduction	29
2.2 Methodology	30
2.3 Validation	33
2.3.1 CFD-AD	33
2.3.2 CFD-AD/BET	35
2.4 Application to Ducted Wind Turbines	38
2.4.1 Phase VI rotor enclosed by the Selig S1223	38
2.5 Conclusions	45

Table of contents

3	Comparison of coupled and uncoupled design strategies for DWTs	47
3.1	Introduction	47
3.2	Description of the CFD-based numerical strategy	49
3.3	Description of the optimization strategy	51
3.4	Results and discussion	53
3.4.1	Uncoupled design	54
3.4.2	Coupled design	57
3.4.3	Comparison between the coupled and uncoupled procedures in terms of blade geometry	61
3.5	Conclusions	61
4	Design of a novel diffuser augmented wind turbine using the Joukowsky rotor	64
4.1	Introduction	64
4.2	Methodology	65
4.2.1	Optimization framework and geometry parametrisation.	68
4.3	Results	71
4.4	Blade geometry reconstruction	75
4.5	Conclusions	77
	Conclusions	81
	Future work	82
	References	82

List of Figures

I.1	World electricity production by source in 2021 (left) and annual increase of wind turbine installed power (right) [78].	1
I.2	Sketch of a ducted wind turbine.	2
1.1	Sketch of a ducted wind turbine.	10
1.2	Computational domain (for the sake of clarity the representation of the actual mesh is coarsened skipping two grid lines out of three)	11
1.3	Detailed view of the blade-to-blade grid for a constant value of the spanwise-index of the structured mesh.	11
1.4	Detailed view of the meridional mesh around different ducts.	12
1.5	Close-up view of the hub mesh.	12
1.6	Grid independence test quantities for the Phase VI rotor ducted in a Selig 1223.	14
1.7	Blade wall pressure coefficient at different span stations: $V_\infty = 7m/s$ ($\lambda = 5.4$).	15
1.8	Blade wall pressure coefficient at different span stations: $V_\infty = 10m/s$ ($\lambda = 3.8$).	15
1.9	Pressure coefficient at different span stations: $V_\infty = 15m/s$ ($\lambda = 2.5$). . .	15
1.10	Blade pressure-force coefficients at different wind speeds.	16
1.11	Integral parameters of the NREL Phase VI for three different values of the wind speed: $7m/s$ ($\lambda = 5.4$), $10m/s$ ($\lambda = 3.8$) and $15m/s$ ($\lambda = 2.5$). .	16
1.12	Mechanical power curve of DonQi DWT.	17
1.13	Dimensionless mass flow rate at the duct throat in the stand-alone configuration.	18
1.14	Normalized axial velocity contour at the rotor plane.	19
1.15	Azimuthally averaged rotor inlet quantities for the open (solid) and ducted (dashed) cases.	20
1.16	Azimuthally-averaged static pressure coefficient details around the duct. .	21
1.17	Contours of static pressure coefficient along the spanwise direction (left) and wall static pressure coefficient with limiting streamlines (right) . . .	23
1.18	Force linear density distributions at different wind speeds for the open (solid) and ducted (dashed) configurations.	23

List of Figures

1.19	Tip flow details: static pressure coefficient contour on blade surface and entropy contours at several constant azimuthal coordinate ($\theta = const.$) planes.	24
1.20	Integral parameters in open and ducted configurations.	25
1.21	Contours of the azimuthally-averaged normalized axial velocity for the open (bottom) and ducted (top) wind turbine.	27
1.22	Contours of the azimuthally-averaged normalized radial velocity for the open (bottom) and ducted (top) wind turbine.	27
1.23	Contours of the azimuthally-averaged normalized tangential velocity for the open (bottom) and ducted (top) wind turbine.	28
2.1	Workflow of the CFD-AD/BET methodology.	31
2.2	Hub and duct mesh details.	32
2.3	Comparison of the CFD-AD open wind turbine performance with the AMT equation.	34
2.4	Comparison of the CFD-AD ducted wind turbine performance with the AMT equation.	34
2.5	Thrust and power coefficient of the open rotor NREL Phase VI.	36
2.6	Linear density distribution of axial and tangential forces for the open rotor NREL Phase VI.	36
2.7	Thrust and power coefficient of the open rotor MEXICO.	37
2.8	Linear density distribution of axial and tangential forces for the open rotor MEXICO.	38
2.9	PIV and CFD-AD/BET velocity distributions downstream of the rotor ($z/R = 0.13$) for different wind speed.	38
2.10	Thrust and power coefficient of the rotor NREL Phase VI enclosed within the Selig S1223.	39
2.11	Linear density distribution of axial and tangential forces for the open rotor NREL Phase VI enclosed within the Selig S1223.	40
2.12	Effects of the c_3 constant on the linear density distribution of axial and tangential forces for the open rotor NREL Phase VI enclosed within the Selig S1223.	40
2.13	Effects of the c_3 constant on the thrust and power coefficient of the rotor NREL Phase VI enclosed within the Selig S1223.	41
2.14	Velocity distribution for the Phase VI rotor enclosed within the Selig S1223.	42
2.15	Static pressure coefficient on the Selig S1223 duct surface for 4, 6 and 8 m/s.	42
2.16	Power curve of the DonQi urban windmill.	43
2.17	Linear density distribution of axial and tangential forces for the DonQi urban windmill.	44
2.18	Axial (left), radial (middle) and tangential (right) velocity component at $z/R_{rot} = 1$	44

List of Figures

2.19	Static pressure coefficient on the DonQi urban windmill duct surface for 5 and 7 m/s	45
3.1	Sketch of the mesh for 2D simulations (not-to-scale): unstructured (gray), structured (red) and boundary-layer inflation (green) blocks	49
3.2	Mesh details.	50
3.3	Optimization workflow for DWT optimization.	52
3.4	Sketch of the baseline DAWT.	53
3.5	Convergence history for the duct shape optimization in the empty configuration (left) and the actual configurations (right).	55
3.6	Distribution of the duct static pressure coefficient of the uncoupled design with and without the rotor.	56
3.7	Flow field differences between the uncoupled optimized configuration, without the rotor (top) and with the rotor (bottom).	57
3.8	Convergence history for the coupled DAWT optimization (left) and the actual configurations (right).	58
3.9	Flow-field contours of the baseline (half top) and optimized (half bottom) configurations	59
3.10	Distribution of the duct wall static pressure coefficient of the baseline and the coupled optimized geometry and static pressure contours near the leading edge.	60
3.11	Radial distribution of rotor parameters normalized by their reference values.	62
3.12	Isometric (left), $r - z$ (middle) and $r - \theta$ (right) views for the coupled (top) and uncoupled (bottom) designs.	62
4.1	Sketch of the multi-block mesh for 2D simulations (not-to-scale).	66
4.2	Mesh details.	67
4.3	Duct shape parametrization with design variables, camber line (dash-dotted black) and control polygons of the pressure (blue) and suction (red) sides.	69
4.4	Design variables for the rotor-duct coupling.	70
4.5	Optimization workflow.	70
4.6	Duct wall static pressure coefficient (a) and contours of static pressure coefficient near the duct leading edge (b) for the baseline (top) and the optimized (bottom) configurations	71
4.7	Contours for baseline (top) and optimized (bottom) geometries.	73
4.8	Velocity distributions at disk plane.	74
4.9	Linear density distributions of the forces exerted by the actuator disk.	74
4.10	Blade element forces and geometrical parameters.	75
4.11	Blade chord (top left) and pitch (top right) distributions, and $r - \theta$ (top middle), isometric (bottom left) and $r - z$ views of the DWT.	77

List of Tables

1.1	Some of the most recent works adopting the simplified design procedure relying on the ducting of an open-rotor into an annular wing.	9
1.2	Mesh size for the analysed geometries.	13
3.1	Parameters for the baseline and optimized configurations.	54
4.1	Design parameters and performance for the baseline and the optimized geometries.	72

Nomenclature

Acronyms

CP	control points of a Beziér curve
2D	two-dimensional
3D	three-dimensional
AD	actuator disk
AMT	axial momentum theory
BE/M-T	blade-element/momentum-theory
CFD	computational fluid dynamics
DAWT	diffuser augmented wind turbine
DWT	ducted wind turbine
EXP	experimental data
FSP	front stagnation point
LE	leading Edge
MT	momentum theory
OWT	open wind turbine
PIV	particle image velocimetry
PS	pressure Side
QUICK	quadratic upstream interpolation for convective kinematics
rpm	revolutions per minute
SQP	sequential quadratic programming
SS	suction Side

Nomenclature

TE	trailing Edge
UDF	user defined function

Greek Symbols

α_{LE}, α_{TE}	duct metal angles at LE and TE
β	relative flow angle at rotor inlet
γ	duct stagger angle
λ	tip speed ratio
Ω	rotational speed
ϕ	flow angle
ρ	fluid density
σ	solidity
τ_D	duct thrust ratio
θ	tangential coordinate
θ_P	pitch angle
$\hat{\tau}$	dimensionless tip gap
c_l, c_d	lift and drag coefficient of 2D profile

Roman Symbols

$\Delta \hat{H}$	dimensionless disk load
\dot{m}	mass flow rate
$\langle \hat{v}_{z,d} \rangle$	dimensionless area-averaged axial velocity at disk plane
\mathcal{J}	objective function
\tilde{z}	normalized duct axial coordinate
\vec{x}	design variables vector
\vec{x}_c	design variables vector for the coupled strategy
\vec{x}_u	design variables vector for the uncoupled strategy
\hat{c}	dimensionless chord
\hat{r}	dimensionless radial coordinate

Nomenclature

$\widehat{v}_z, \widehat{v}_\theta, \widehat{v}_r$	dimensionless axial, tangential and radial velocity components
\widehat{v}_θ^+	dimensionless tangential velocity right after the disk plane
$\widehat{v}_{z,d}$	dimensionless axial velocity at disk plane
\widehat{z}	dimensionless axial coordinate
\widehat{z}_d	dimensionless axial position of the disk
\widehat{z}_{LE}	dimensionless axial position of the duct LE
a, a'	axial and tangential induction factors
$A_{rot} A_{exit}$	rotor and frontal swept area
B	rotor blade count
c	chord
c_D	duct chord
c_l, c_d	lift and drag coefficient of the 2D airfoils
C_n, C_t	normal-to-chord and chord-wise pressure-force coefficients
C_P	power coefficient based on rotor area
$C_T, C_{T,R}, C_{T,D}$	overall, rotor and duct thrust coefficient
$c_{D,ax}$	duct axial chord
$C_{P,ex}$	power coefficient based on the frontal area
$C_{press,D}$	duct static pressure coefficient
C_{press}	static pressure coefficient
d_{PS}, d_{SS}	duct control point of PS and SS curves
f_z, f_θ	axial and tangential body forces
$F_z F_t$	axial and tangential force linear density
k	dimensionless kinematic momentum
P	power
p	static pressure
Q	torque
r_{LE}	duct radius at LE

Nomenclature

R_{rot}, r_{hub}	rotor and hub radii
T, T_R, T_D	overall, rotor and duct thrust
v_z, v_θ, v_r	axial, tangential and radial velocity components
w_∞	relative velocity
w_{LE}	duct wedge angle at LE
x, y	chord-wise and normal-to-chord dimensionless profile coordinates
z, r	axial and radial coordinates

Subscripts

∞	upstream infinity state
D	duct
R	rotor

Introduction

Nowadays, wind energy is at the second place of the renewable production rank and produces more energy of all the remaining non-fossil sources combined. In Europe, 16% of the electricity load is covered by wind energy and it is expected to reach 50% by 2050 with 1300GW of installed power. Although the majority of installed power

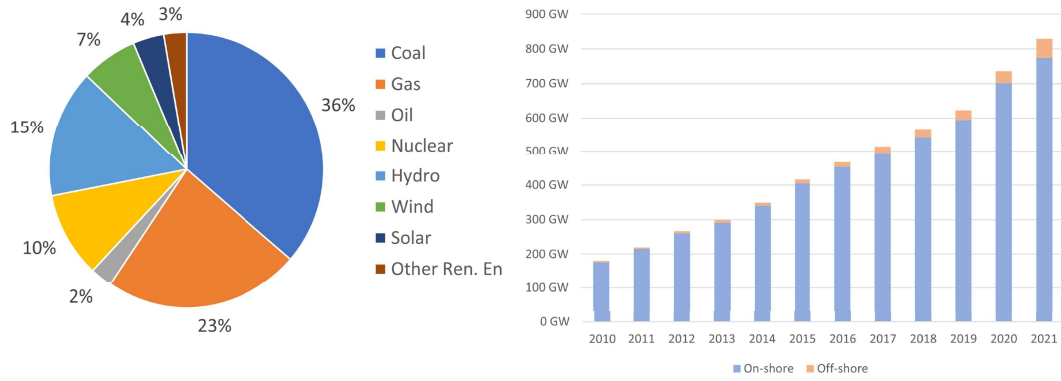


Figure I.1: World electricity production by source in 2021 (left) and annual increase of wind turbine installed power (right) [78].

is concentrated in on-shore wind farms, off-shore and small-scale devices are gradually increasing at a rate larger than the land ones. Indeed, the land-based wind production can only be raised by installing more wind turbines/wind-farms or by increasing the rotor size. However, the large size of these devices involves a non-negligible impact on the surrounding landscape. Besides the new off-shore wind farms, small-scale wind-energy harvesting systems are spreading due to the advantage of their direct installation near the end-user local grids. By simple analysis of the axial momentum theory, it is easily proven that the open rotor can not extract all the power provided by the wind. Expressed in dimensionless terms, there is an upper bound of approximatively 59%, which is the well-known Betz-Joukowski limit. In this scenario, a very promising solution to overcome some of the open rotor limitations is based on enclosing the rotor within an external duct, whose shape could be axisymmetric or not, namely the Ducted Wind Turbines (DWTs). The duct needs to provide a thrust vector concordant with the rotor thrust to increase the rotor power coefficient, which is typically achieved with

Introduction

a divergent or convergent-divergent nozzle. In Figure I.2 the sketch of a DAWT is reported, where the duct is an aerodynamically shaped profile and the rotor is replaced by the red disk. Considering that the flow-field is parallel to the rotational axis, the L

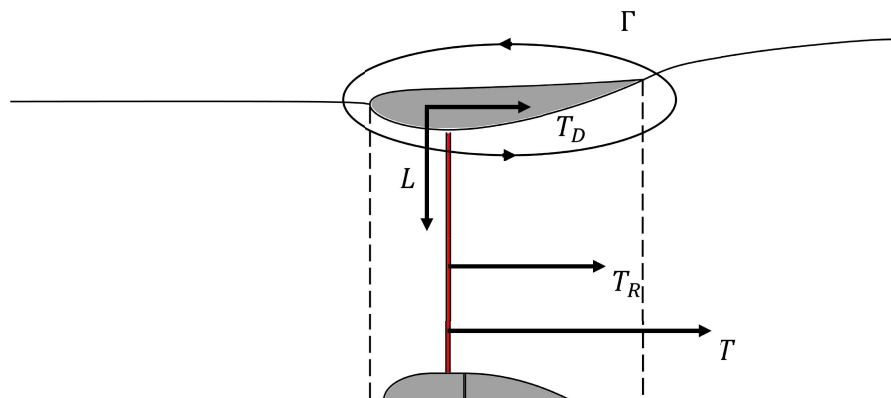


Figure I.2: Sketch of a ducted wind turbine.

and T_D vectors represent the lift and drag (or thrust) forces acting on the duct, while T_R and $T = T_R + T_D$ are the rotor and total thrust, respectively. With a properly designed profile shape, the circulation Γ is the main responsible of the increasing in the mass flow rate swallowed by the rotor, which ultimately will lead to a higher extracted power. The presence of the duct, especially when the convergent-divergent configuration is used, reduces the cut-in speed and reduces the sensitivity to yaw angles. Additionally, higher safety is ensured in case of rotor failure, the tip losses are reduced and the level of noise is also lowered. However, the additional load acting on the DWT supports implies higher structural requirements and overall costs.

The flow past a DWT is completely different from the one past an open rotor. Indeed, the captured area at infinity upstream is increased by the presence of the duct, a counter-intuitive fact which strongly depends on the rotor load. The aim of the blading system is to extract energy from the ingested stream-tube by varying its tangential component all over the span. Near the rotor tip, the flow is pushed within the technological gap between the blade and the duct by the pressure difference acting on the pressure and suction sides, without being turned, with no work extracted. Additionally, it rolls up and generates the so-called tip-vortex, which sheds downstream following a helicoidal path. Downstream the rotor, the flow experiences the diffusion imposed by the divergent section of the duct. The tip-vortex may interact with the duct inner-surface boundary layer, re-energizing it, and eventually delaying or avoiding any separation. Finally, far behind the rotor, a strong mixing involves the trailing edge wake, the tip-vortex and the free-shear layer. From this qualitative description of the phenomena, it is clear that the duct-rotor interaction is a very key-point in the analysis of DWTs performance, and properly taking it into account during the design phase is even more challenging.

Blade resolved analysis of Ducted Wind Turbines

The study of ducted wind turbines via blade-resolved simulations is one of the most accurate approach. Specifically, a fluid domain is created around the 3-D geometry of the DWT, which is typically divided into a large number of finite volumes. On the latter, the discretized form of the Navier-Stokes (NS) equations are solved by standard PDE numerical techniques. The level of accuracy is defined by choice of the methodology to be used in the numerical solution of the equations. At the current state of the art, Direct Numerical Simulations of DWTs have not been performed yet, due to the Reynolds number constraints on the scale resolution. Nevertheless, several researches analysed the performance of ducted wind turbines by means of Large Eddy Simulations (LES), with the main goal of understanding the mixing in the rotor wake and the associated aerodynamic noise. Avallone et al. [14] performed Lattice-Boltzmann Very Large Eddy Simulations of a ducted wind turbine aiming at assessing the effects of the tip gap on the overall performance. They found out that the flow separation on the duct inner-side shifts towards the trailing edge as the gap value increases, due to its interaction with the boundary layer. In a successive work [28], the behaviour of a DWT [31] has been investigated at different inflow angles. The outcome of this study demonstrated that, contrarily to the open case, the extracted power is only slightly affected by the inflow yaw angle.

A further simplification of the analysis method can be made by considering the Reynolds-Averaged Navier-Stokes (RANS) equations and their unsteady formulation (URANS). As already explained in this section, the flow past a DWT is characterised by a high level of unsteadiness so that the URANS simulations seem to be more appropriate for the investigation of these devices. At a nominal Reynolds number, based on the free stream velocity and chord length, of 10^6 a typical mesh count for a RANS/URANS simulation is between 15 and 20×10^6 points, making this type of analysis rather expensive, also depending on the available computational power, especially if several rotor revolutions are needed to achieve a quasi periodic solution. Therefore, the simplest blade-resolved analysis can be carried out using the steady-state RANS equations and two different approaches exist. A first approach consists in enclosing the rotor within a cylindrical domain virtually rotating within the stationary frame of reference, which is also known as Multiple Reference Frame or Frozen Rotor. By doing so, the rotational effects, as the Coriolis and centrifugal forces, are only acting inside the rotor region. The scalar quantities are conserved across the interfaces of the two domains whereas the velocities are converted to guarantee the local continuity across the shared boundaries. A different approach could be used when, except for the rotor, all the other surfaces are obtained by revolution and no struts, or multiple rows, are considered. This method is also known as the Single Reference Frame, where the rotational terms are activated for all the domain cells. Several research groups employed these approaches to analyse the feasibility of DWTs. Coşoiu et al. [24] investigated the performance improvement of the commercial open rotor SICE-1kW when it's enclosed within an external duct consisting of the NACA 4412 profile. The latter was modified to include a trailing edge appendix,

also known as Gurney flap, conceived to increase the power coefficient at all tip speed ratios. This strategy highlighted a maximum C_P value equal to 2.09 the Betz limit. Wang et al. [75] proposed a novel rotor design by replacing the traditional blades with a multi-blade disk arrangement, while the duct was a simple divergent nozzle constructed with a thin plate. The performance of the ducted rotor turned out to be remarkable, with a power twice the open rotor value. Aranake et al. [11, 13] carried out a wide study to find the best duct cross-section shape for the NREL Phase VI open rotor. Particularly, the Eppler E423, the Selig S1223, a modified NACA0006 and the FX 74-CL5-140 profiles were analysed as isolated components by means of 2D simulations at different angles of attack. The Selig S1223 was selected due to the highest mass flow rate amplification and the higher lift coefficient. Then, the URANS simulations highlighted that the ducted rotor power coefficient overcomes the Betz limit, with an extraordinary augmentation factor equal to 1.91, far larger than the corresponding CFD-AD value. Moreover, they also underlined the effect of the tip-gap flow on the duct inner-surface separation, especially at higher rotational speeds, when the frequency of the helicoidal wake increases. Jafari and Kosasih [37] performed a parametric study of a divergent nozzle as placed around the commercial open rotor AMPAIR 300 Watt micro-wind turbine. As common practice for the diverging nozzles, the considered parameters were the duct exit area, the height of the divergent part, and the length of the diffuser region. The outcome showed that, the higher the diffusion downstream the rotor, the higher the power gain, until the separation on the inner surface causes a neat performance fall. Roshan et al. [50] analysed the effect of a step on the inner surface of a simply diverging duct at several axial locations. In this case, the 3D simulations of the duct were carried out without considering the presence of the rotor and the best configuration was chosen to maximize the averaged velocity at the rotor plane. Once the optimal duct shape was defined, the rotor was included in the analysis and the effects of its axial position were investigated. Among all the possible solutions, the power coefficient assumed the maximum value of 0.9 when the blades are placed at the duct inlet.

An interesting application of ducted wind turbine was proposed by Saeed and Kim [51], who enclosed the NREL Phase VI rotor within an air-bone system, whose original shape was a simple conical diverging nozzle with several fins, needed for stability reasons. However, the unsteady simulations of the system showed that the torque of the ducted configuration was slightly higher than the open one only for a limited range of tip speed ratios. In a successive work [53], a parametric study on the rotor axial position was carried out, showing that the maximum power coefficient of 0.4 was obtained when the blades are placed at the throat location. Then, the simple diverging duct shape was replaced by three different contoured divergent ducts built with the NACA-5415, NACA-9415 and NACA-5425 profiles. The second one, with a tip gap of 1% of the rotor radius, showed higher performance than the other two profiles, reaching a C_P of 0.72. Finally, Saleem and Kim [52] parametrized the 2-D cross-section using the PARSEC method, aiming at maximizing the lift coefficient of the isolated 2D profile. The resulting air-bone DWT outperformed the one based on the NACA-9415 by 20%, with a remarkable maximum power coefficient equal to 1.25. Siavash et al. [63] designed

a new rotor, disregarding the duct presence, and proposed a modular duct, increasing the power coefficient up to 0.35, 50% higher than the open rotor.

Low order models for Ducted Wind Turbines analysis

The first low order models for DWT analysis appeared at the beginning of the previous century with the work of Betz [16], where it was concluded that a ducted rotor can not extract more than 65% of the power of an open wind turbine, with the same frontal area. As a consequence, the interest in these energy harvesting systems was lost and no further configurations were considered. Afterwards, new models were proposed by different researchers with promising results and they could be divided into two main categories, namely those based on the axial momentum theory [25–27, 41, 77] and those based on mechanical energy balances [16, 34, 39, 42, 48, 68]. The axial momentum theory is a widely-spread and effective tool to analyse the performance of a open wind turbine. The flow is assumed to be steady, incompressible, inviscid and axial-symmetric, while the rotor is replaced by an actuator disk of infinitesimal thickness, which applies the same effects of the blades to the fluid. The domain is divided into three main regions, i.e. the stream-tube ingested by the rotor upstream, the stream-tube digested by the rotor downstream and the remaining fluid. Then, continuity and momentum balances are applied to the control volumes and the performance of the turbine are readily evaluated. Particularly, the degree of divergence of the stream-tube strongly depends on the value of the rotor thrust, increasing as the latter increases. Including the duct within the analysis, the main difficulty consists in determining the shape of the ingested stream-tube, which, in this case, depends on the rotor thrust and on the duct thrust. In turn, the latter is not easy to evaluate since it results from the rotor-duct interaction and it can not be evaluated a-priori. The mechanical-energy-based models have the same hypothesis of the previous case. Similarly, the knowledge of the diffusion efficiency and of the velocity induced at the rotor plane are required as input. In conclusion, these two models need the a-priori knowledge of some parameters which cannot be known a-priori, especially when a new design is sought.

Therefore, coupling the actuator disk with the axial-symmetric computations of the flow field via RANS equations is a wide-spread methodology for the analysis of ducted wind turbines. Specifically, the numerical domain contains a disk region, where source terms are activated in the axial and tangential equations, which represent the effect of the pressure jump and the swirl velocity imposed to the fluid by the rotor. Dimensionally, the source terms are forces per unit volume and can be computed by imposing the load at the different radial stations or by coupling the CFD-AD with a BET module. In the last case, the blade cross-sections, twist and chord are already defined, so that the aerodynamic forces can be evaluated and assigned to the local elements along the span. Aranake and Duraisamy [10] used the CFD-AD method to evaluate the performance of DWTs and included the module within an optimization procedure. The PARSEC parametrisation was applied to the duct shape and the extracted power was maximized, obtaining an optimized power coefficient based on the exit area equal to 0.71. Dighe et al. [29] used the CFD-AD to evaluate the effects of applying an aerodynamic appendix to

Introduction

the duct trailing edge, the so-called Gurney flap, showing that the separated flow behind the duct generates a low-pressure region, which increases the mass flow rate swallowed by the rotor. In a successive work [30], an investigation of the performance for different duct shapes and disk loads has been carried out via CFD-AD, showing that the best performance were obtained with a high-cambered duct. Moreover, they found out that the extracted power increases as the velocity at the rotor plane increases, even if the duct upper surface is completely separated. Venters et al. [73] optimized the configuration of a ducted wind turbine, whose duct shape was based on the Eppler profile. Particularly, the optimal duct stagger angle, tip gap, axial position and disk load was sought to maximize the power coefficient first, and the power coefficient based on the frontal area, then. Khamlaj and Rumpfkeil [38] parametrised the duct geometry, the rotor twist and chord distributions by several Beziér curves and used their control points as design variables to maximize the power output and minimizing the rotor thrust, obtaining a power coefficient value equal to 0.923. Saleem and Kim [52] optimized the parametrized shape of the duct to maximize the lift coefficient of the isolated profile. The resulting profile was then coupled with the NREL Phase VI rotor, reporting a maximum power coefficient of 1.25. Alkhabbaz et al. [6] carried out the design of a ducted wind turbine by optimizing the duct and the rotor in an uncoupled fashion. Indeed, the averaged velocity at the rotor plane induced by the duct alone was increased and, then, the Glauert optimum theory was employed for the rotor design. A power coefficient equal to 0.6, computed by the blade-resolved simulations was ultimately achieved. Finally, Leloudas et al. [40] optimized the duct alone by increasing the velocity at the disk plane and minimizing the thrust coefficient of the duct, without including the rotor within the simulations, resulting in a 21% increase in the axial velocity at the disk, with a 45% reduction of the duct thrust.

Motivation

The overview presented in the previous sections highlights that the flow past a ducted wind turbine is far more complicated than the one past an open wind turbine. The strong duct-rotor interaction determines the degree of increase in the device performance and can not be easily reproduced by simple models. Therefore, the design of DAWT is typically performed through an iterative procedure, which aims at finding the best duct shape and the best rotor load, contemporarily. Due to the high computational costs of the high-fidelity blade-resolved methodologies, a design based on 3D shape-optimization is prohibitive, unless high-performance computers are used. As a consequence, CFD-AD based methods are typically employed. These designs neglect some of the loss mechanisms associated with the real rotor geometry and typically over-estimate the device performance. A quite common practice relies on the optimization of the duct alone, without considering the rotor, while the rotor is only designed afterwards or an already existing rotor is employed. This leads, at best, to suboptimal designs. Additionally, most of the research works do not analyse or assess the impact of such assumptions, which also prevent to overcome the Betz limit. Indeed, the uncoupled design involves modifications of the operating point once the rotor is introduced within the duct, typically leading to

Introduction

the modification of the duct front stagnation point or a change of the incidence on the rotor blades, which modifies the related aerodynamic loads. Furthermore, most of the CFD-AD designs do not take into account the end-blade corrections, needed for a finite blade rotor, or they use the same formula of the open rotors, as the Prandtl corrections.

The goal of this thesis is to give further insights on the design methods for ducted wind turbines by

- analysing the limitations of ducting an existing open rotor or ducting a rotor designed to work in open configuration,
- assessing the validity of the CFD-AD simulations for DWTs against experimental and blade-resolved simulations data,
- investigating the two most common design strategies for ducted rotor, i.e. the uncoupled and coupled methods.

Finally, all the understandings of these investigations are included within a design module specifically built for ducted wind turbines.

The first chapter analyses the limitations of enclosing an already existing rotor, namely the NREL Phase VI rotor, within the Selig S1223, whose configuration has been chosen to maximize the swallowed mass flow. The analysis is carried out via 3D blade-resolved simulations and, once the methodology is validated using the available experimental data, the investigation of the DWT is performed by analysing the local flow-field quantities, the blade force distributions and the integral coefficients at different tip speed ratios.

The second chapter is dedicated to the assessment of the CFD-AD method, coupled with a BET module, as applied to ducted wind turbine. The main goal is to understand the level of accuracy reached by the model since the blade unloading towards the blade tip differs from the open case. Indeed, this correction has an important role in determining the effects of the tip-vortex on the duct inner-surface boundary layer, i.e. the possible delay of the flow separation.

The third chapter deals with the investigation of two wide-spread DWT design procedures, namely the uncoupled and the coupled one. In both cases, the CFD-AD is employed as analysis method and the Joukowsky rotor is considered for the source terms evaluation, which is also known as free-vortex velocity distributions, while the duct shape is the Selig S1223. The choice of the constant load along the span is based on the results obtained for open rotors, which showed better results compared to all the other methods. In the uncoupled design approach, the duct geometry is optimized to maximize the ingested mass flow and, then, the maximum power coefficient based on the exit area is sought by modifying the disk load. Contrariwise, the coupled design foresees the determination of the maximum power coefficient based on the exit area by considering the duct geometries features and the disk load as design variables, contemporarily. Finally, in the fourth chapter, the duct shape is completely parametrized and, based on the results of the previous chapter, the coupled methodology is applied to design a novel and more efficient ducted wind turbine.

References

- [1] Abe, K. and Ohya, Y. “An investigation of flow fields around flanged diffusers using CFD”. In: *Journal of wind engineering and industrial aerodynamics* 92.3 (2004), pp. 315–330.
- [2] Agha, A., Chaudhry, H. N., and Wang, F. “Determining the augmentation ratio and response behaviour of a diffuser augmented wind turbine (DAWT)”. In: *Sustainable Energy Technologies and Assessments* 37 (2020), p. 100610.
- [3] Ali, Q. S. and Kim, M.-H. “Design and performance analysis of an airborne wind turbine for high-altitude energy harvesting”. In: *Energy* 230 (2021), p. 120829.
- [4] Ali, Q. S. and Kim, M.-H. “Power conversion performance of airborne wind turbine under unsteady loads”. In: *Renewable and Sustainable Energy Reviews* 153 (2022), p. 111798.
- [5] Ali, Q. S. and Kim, M.-H. “Quantifying impacts of shell augmentation on power output of airborne wind energy system at elevated heights”. In: *Energy* 239 (2022), p. 121839.
- [6] Alkhabbaz, A., Yang, H.-S., Tongphong, W., and Lee, Y.-H. “Impact of compact diffuser shroud on wind turbine aerodynamic performance: CFD and experimental investigations”. In: *International Journal of Mechanical Sciences* 216 (2022), p. 106978.
- [7] ANSYS. *Ansys Fluent Customization Manual*. 2021.
- [8] ANSYS. *Fluent Theory Guide*. 2021.
- [9] ANSYS. *ANSYS Fluent User’s Guide*. ANSYS Inc. 2021.
- [10] Aranake, A. and Duraisamy, K. “Aerodynamic optimization of shrouded wind turbines”. In: *Wind Energy* 20.5 (2016), pp. 877–889.
- [11] Aranake, A., Lakshminarayan, V., and Duraisamy, K. “Assessment of Transition Model and CFD Methodology for Wind Turbine Flows”. In: *42nd AIAA Fluid Dynamics Conference and Exhibit*. American Institute of Aeronautics and Astronautics, 2012.
- [12] Aranake, A., Lakshminarayan, V., and Duraisamy, K. “Computational Analysis of Shrouded Wind Turbine Configurations”. In: *51st AIAA Aerospace Sciences Meeting including the New Horizons Forum and Aerospace Exposition*. American Institute of Aeronautics and Astronautics, 2013.

References

- [13] Aranake, A., Lakshminarayan, V., and Duraisamy, K. “Computational analysis of shrouded wind turbine configurations using a 3-dimensional RANS solver”. In: *Renewable Energy* 75 (2015), pp. 818–832.
- [14] Avallone, F., Ragni, D., and Casalino, D. “On the effect of the tip-clearance ratio on the aeroacoustics of a diffuser-augmented wind turbine”. In: *Renewable Energy* 152 (2020), pp. 1317–1327.
- [15] Betz, A. “Das Maximum der theoretisch möglichen Ausnützung des Windes durch Windmotoren”. In: *Zeitschrift für das gesamte Turbinenwesen* 26 (1920), pp. 307–309. (English translation: Betz A., The maximum of the theoretically possible exploitation of wind by means of a wind motor. *Wind Engineering*, 37(4): 441-6, 2013).
- [16] Betz, A. “Energieumsetzungen in venturidüsen”. In: *Naturwissenschaften* 17.10 (1929), pp. 160–164.
- [17] Bontempo, R., Carandente, R., and Manna, M. “A design of experiment approach as applied to the analysis of diffuser-augmented wind turbines”. In: *Energy Conversion and Management* 235 (2021), p. 113924.
- [18] Bontempo, R. and Manna, M. “Diffuser augmented wind turbines: Review and assessment of theoretical models”. In: *Applied Energy* 280 (2020), p. 115867.
- [19] Bontempo, R. and Manna, M. “Effects of the duct thrust on the performance of ducted wind turbines”. In: *Energy* 99 (2016), pp. 274–287.
- [20] Bontempo, R. and Manna, M. “On the potential of the ideal diffuser augmented wind turbine: an investigation by means of a momentum theory approach and of a free-wake ring-vortex actuator disk model”. In: *Energy Conversion and Management* 213 (2020), p. 112794.
- [21] Bontempo, R. and Manna, M. “Performance analysis of open and ducted wind turbines”. In: *Applied Energy* 136 (2014), pp. 405–416.
- [22] Bontempo, R. and Manna, M. “The Joukowsky rotor for diffuser augmented wind turbines: design and analysis”. In: *Energy Conversion and Management* 252 (2022), p. 114952.
- [23] Burton, T, Sharpe, D, Jenkins, N, and Bossanyi, E. *Wind energy handbook*. John Wiley & Sons, 2001.
- [24] Coşoiu, C. I., Damian, R. M., Degeratu, M., Georgescu, A., and Hlevca, D. “Numerical study on the efficiency between the ducted and the free stream rotor of a horizontal axis wind turbine”. In: *Proceedings of EWEA Europe’s Premier Wind Energy Event, Brussels* (2011), pp. 14–17.
- [25] de Vries, O. *Fluid dynamic aspects of wind energy conversion*. AGARD No.243, 1979.
- [26] Dick, E. “Momentum analysis of wind energy concentrator systems”. In: *Energy conversion and management* 24.1 (1984), pp. 19–25.

References

- [27] Dick, E. “Power limits for wind energy concentrator systems”. In: *Wind Engineering* (1986), pp. 98–115.
- [28] Dighe, V. V., Avallone, F., and Bussel, G. van. “Effects of yawed inflow on the aerodynamic and aeroacoustic performance of ducted wind turbines”. In: *Journal of Wind Engineering and Industrial Aerodynamics* 201 (2020), p. 104174.
- [29] Dighe, V. V., Avallone, F., Tang, J., and Bussel, G. van. “Effects of gurney flaps on the performance of diffuser augmented wind turbine”. In: *35th Wind Energy Symposium*. 2017, p. 1382.
- [30] Dighe, V. V., Oliveira, G. de, Avallone, F., and Bussel, G. van. “Towards improving the aerodynamic performance of a ducted wind turbine: A numerical study”. In: *Journal of Physics: Conference Series* 1037 (2018), p. 022016.
- [31] Dighe, V. V., Oliveira, G., Avallone, F., and Bussel, G. J. W. “Characterization of aerodynamic performance of ducted wind turbines: A numerical study”. In: *Wind Energy* 22.12 (2019), pp. 1655–1666.
- [32] Ding, C., Zhang, B., Liang, C., Visser, K., and Yao, G. “High-Order Large Eddy Simulations of a Wind Turbine in Ducted and Open-Rotor Configurations”. In: *Journal of Fluids Engineering* 145.2 (2023), p. 021201.
- [33] Drela, M. “XFOIL: An analysis and design system for low Reynolds number airfoils”. In: *Low Reynolds number aerodynamics*. Springer, 1989, pp. 1–12.
- [34] Foreman, K., Gilbert, B., and Oman, R. “Diffuser augmentation of wind turbines”. In: *Solar Energy* 20.4 (1978), pp. 305–311.
- [35] Hand, M. M., Simms, D., Fingersh, L., Jager, D., Cotrell, J., Schreck, S., and Larwood, S. *Unsteady aerodynamics experiment phase VI: wind tunnel test configurations and available data campaigns*. Tech. rep. National Renewable Energy Lab., Golden, CO.(US), 2001.
- [36] Hashem, I., Mohamed, M. H., and Hafiz, A. A. “Numerical investigation of small-scale shrouded wind turbine with a brimmed diffuser”. In: *Proceedings of ICFD12: 12th International Conference of Fluid Dynamics, Le Méridien Pyramids Hotel, Egypt*. Vol. 5003. 2016.
- [37] Jafari, S. and Kosasih, B. “Flow analysis of shrouded small wind turbine with a simple frustum diffuser with computational fluid dynamics simulations”. In: *Journal of Wind Engineering and Industrial Aerodynamics* 125 (2014), pp. 102–110.
- [38] Khamlaj, T. A. and Rumpfkeil, M. “Optimization study of shrouded horizontal axis wind turbine”. In: *2018 wind energy symposium*. 2018, p. 0996.
- [39] Lawn, C. J. “Optimization of the power output from ducted turbines”. In: *Proceedings of the Institution of Mechanical Engineers, Part A: Journal of Power and Energy* 217.1 (2003), pp. 107–117.
- [40] Leloudas, S. N., Lygidakis, G. N., Eskantar, A. I., and Nikolos, I. K. “A robust methodology for the design optimization of diffuser augmented wind turbine shrouds”. In: *Renewable Energy* 150 (2020), pp. 722–742.

References

- [41] Lewis, R., Williams, J., and Abdelghaffar, M. “A theory and experimental investigation of ducted wind turbines”. In: *Wind Engineering* 1.2 (1977), pp. 104–125.
- [42] Lilley, G. and Rainbird, A. *A preliminary report on the design and performance of ducted windmills*. Tech. rep. College of Aeronautics, Cranfield, 1956.
- [43] Manna, M. and Tuccillo, R. “Improving the aero-thermal characteristics of turbomachinery cascades”. In: *J. Turbomach.* 125.2 (2003), pp. 317–327.
- [44] Menter, F. R., Kuntz, M., and Langtry, R. “Ten years of industrial experience with the SST turbulence model”. In: *Turbulence, heat and mass transfer* 4.1 (2003), pp. 625–632.
- [45] Noorollahi, Y., Ghanbari, S., and Tahani, M. “Numerical analysis of a small ducted wind turbine for performance improvement”. In: *International Journal of Sustainable Energy* 39.3 (2019), pp. 290–307.
- [46] Noronha, N. P. and Krishna, M. “Design and analysis of micro horizontal axis wind turbine using MATLAB and QBlade”. In: *International Journal of Advanced Science and Technology* 29.10S (2020), pp. 8877–85.
- [47] Noronha, N. P. and Munishamaih, K. “Performance assessment of a balloon assisted micro airborne wind turbine system”. In: *Energy Harvesting and Systems* 8.2 (2021), pp. 63–71.
- [48] Oman, R. and Foreman, K. “Advantages of the diffuser-augmented wind turbine”. In: *NASA. Lewis Res. Center Wind Energy Conversion Systems* (1973).
- [49] Regodeseves, P. G. and Morros, C. S. “Unsteady numerical investigation of the full geometry of a horizontal axis wind turbine: Flow through the rotor and wake”. In: *Energy* 202 (2020), p. 117674.
- [50] Roshan, S. Z., Alimirzazadeh, S., and Rad, M. “RANS simulations of the stepped duct effect on the performance of ducted wind turbine”. In: *Journal of Wind Engineering and Industrial Aerodynamics* 145 (2015), pp. 270–279.
- [51] Saeed, M. and Kim, M.-H. “Aerodynamic performance analysis of an airborne wind turbine system with NREL Phase IV rotor”. In: *Energy conversion and management* 134 (2017), pp. 278–289.
- [52] Saleem, A. and Kim, M.-H. “Aerodynamic performance optimization of an airfoil-based airborne wind turbine using genetic algorithm”. In: *Energy* 203 (2020), p. 117841.
- [53] Saleem, A. and Kim, M.-H. “Effect of rotor axial position on the aerodynamic performance of an airborne wind turbine system in shell configuration”. In: *Energy Conversion and Management* 151 (2017), pp. 587–600.
- [54] Saleem, A. and Kim, M.-H. “Effect of rotor tip clearance on the aerodynamic performance of an aerofoil-based ducted wind turbine”. In: *Energy Conversion and Management* 201 (2019), p. 112186.

References

- [55] Saleem, A. and Kim, M.-H. “Performance of buoyant shell horizontal axis wind turbine under fluctuating yaw angles”. In: *Energy* 169 (2019), pp. 79–91.
- [56] Schepers, J., Boorsma, K., Cho, T., Gomez-Iradi, S., Schaffarczyk, P., Shen, W., Lutz, T., Stoevesandt, B., Schreck, S., Micallef, D., et al. *Analysis of Mexico wind tunnel measurements. Final report of IEA Task 29, Mexnext (Phase 1)*. Tech. rep. 2012.
- [57] Schittkowski, K. “NLPQL: A FORTRAN subroutine solving constrained nonlinear programming problems”. In: *Annals of operations research* 5.2 (1986), pp. 485–500.
- [58] Selig, M. S., Guglielmo, J. J., Broeren, A. P., and P., G. *Summary of low speed airfoil data, Vol. 1*. Virgini Beach, Virginia 23451, USA: SoarTech publications, 1995.
- [59] Selig, M. S., Guglielmo, J. J., Broeren, A. P., and P., G. *Summary of low speed airfoil data, Vol. 3*. Virgini Beach, Virginia 23451, USA: SoarTech publications, 1995.
- [60] Shen, W. Z., Mikkelsen, R., Sørensen, J. N., and Bak, C. “Tip loss corrections for wind turbine computations”. In: *Wind Energy: An International Journal for Progress and Applications in Wind Power Conversion Technology* 8.4 (2005), pp. 457–475.
- [61] Shives, M and Crawford, C. “Computational analysis of ducted turbine performance”. In: *Proceedings of the 3rd International Conference on Ocean Energy, Bilbao, Spain*. 2010.
- [62] Siavash, N. K., Ghobadian, B., Najafi, G., Rohani, A., Tavakoli, T., Mahmoodi, E., Mamat, R., et al. “Prediction of power generation and rotor angular speed of a small wind turbine equipped to a controllable duct using artificial neural network and multiple linear regression”. In: *Environmental research* 196 (2021), p. 110434.
- [63] Siavash, N. K., Najafi, G., Hashjin, T. T., Ghobadian, B., and Mahmoodi, E. “An innovative variable shroud for micro wind turbines”. In: *Renewable Energy* 145 (2020), pp. 1061–1072.
- [64] Siavash, N. K., Najafi, G., Tavakoli, T., Ghobadian, B., and Mahmoodi, E. “An investigation on performance of shrouding a small wind turbine with a simple ring in a wind tunnel”. In: *Journal of Renewable Energy and Environment* 4.4 (2017), pp. 49–56.
- [65] Song, K., Wang, W.-Q., and Yan, Y. “Numerical and experimental analysis of a diffuser-augmented micro-hydro turbine”. In: *Ocean Engineering* 171 (2019), pp. 590–602.
- [66] Sørensen, J. N. “CFD Modeling of wind turbines and wind turbine wakes”. In: *Aerodynamics of Wind Turbines: State of the Art and Future Perspectives. The von Karman Institute for Fluid Dynamics - Lecture Series*. Sint-Genesius-Rode, Belgium, 2022.

References

- [67] Sørensen, J. N. *General Momentum Theory for Horizontal Axis Wind Turbines*. Springer, 2015.
- [68] Sorribes-Palmer, F., Sanz-Andres, A., Ayuso, L., Sant, R., and Franchini, S. “Mixed CFD-1D wind turbine diffuser design optimization”. In: *Renewable Energy* 105 (2017), pp. 386–399.
- [69] ten Hoopen, P. “An experimental and computational investigation of a diffuser augmented wind turbine”. MA thesis. Delft University of Technology, 2009.
- [70] van Dorst, F. “An Improved Rotor Design for a Diffuser Augmented Wind Turbine”. MA thesis. Delft University of Technology, 2011.
- [71] van Kuik, G. A. M. “Joukowski actuator disc momentum theory”. In: *Wind Energy Science* 2.1 (2017), pp. 307–316.
- [72] Vaz, J. R. P. and Wood, D. H. “Aerodynamic optimization of the blades of diffuser-augmented wind turbines”. In: *Energy Conversion and Management* 123 (2016), pp. 35–45.
- [73] Venters, R., Helenbrook, B. T., and Visser, K. D. “Ducted wind turbine optimization”. In: *Journal of Solar Energy Engineering* 140.1 (2018).
- [74] Viterna, L. A. and Janetzke, D. C. *Theoretical and experimental power from large horizontal-axis wind turbines*. Tech. rep. National Aeronautics and Space Administration, Cleveland, OH (USA), 1982.
- [75] Wang, J., Piechna, J., and Müller, N. “Computational Fluid Dynamics Investigation of a Novel Multiblade Wind Turbine in a Duct”. In: *Journal of Solar Energy Engineering* 135.1 (2012).
- [76] Werle, M. J. “An enhanced analytical model for airfoil-based shrouded wind turbines”. In: *Wind Energy* (2020).
- [77] Werle, M. J. and Presz, W. M. “Ducted wind/water turbines and propellers revisited”. In: *Journal of Propulsion and Power* 24.5 (2008), pp. 1146–1150.
- [78] *World Economic Forum*. <https://www.weforum.org/agenda/2022/08/electricity-capacity-power-renewable-energy>. Accessed: 2023-01-07.
- [79] Yakhot, V., Orszag, S. A., Thangam, S., Gatski, T. B., and Speziale, C. G. “Development of turbulence models for shear flows by a double expansion technique”. In: *Physics of Fluids A: Fluid Dynamics* 4.7 (1992), pp. 1510–1520.